https://doi.org/10.5194/egusphere-2025-3803
Preprint. Discussion started: 18 September 2025

Coupled simulation of landslide, tsunami, and ground deformation for the 2017 Nuugaatsiaq event in Greenland

Hideo Aochi[1], Masumi Yamada[2], Tung-Cheng Ho[2], Gonéri Le Cozannet[3], Arno Christian Hammann[4], Ruth Mottram[5]

[1]Direction of Energy, BRGM, Orléans 45060, France
[2]Disaster Prevention Research Institute, Kyoto University, Uji, 611-0011, Japan
[3]Direction of Risks, BRGM, Orléans 45060, France
[4]Asiaq Greenland Survey, Nuuk, 3900, Greeland
[5]Danish Meteorological Institute, Copenhagen, DK-2100, Denmark

Correspondence to: Hideo Aochi (h.aochi@brgm.fr, aochi.hideo@gmail.com)

Abstract. We investigated the entire sequence of the tsunami event led by a massive landslide on June 17, 2017, in Karrat Fjord, near Nuugaatsiaq village, western Greenland to understand the causality of this cascade mechanism. The seismological analysis from seven stations across Greenland allows to estimate the landslide volume. Then, we conducted sequential simulations, consisting of (1) the landslide's descent into the fjord based on topography, (2) tsunami generation and large-scale propagation, and (3) ground deformation caused by tsunami-induced sea level changes, considering both static and elasto-dynamic solutions. A 1 m-height of sea level change may lead to a ground deformation up to 0.1 – 1.0 mm along the coastline, and this can be detected by a seismogram. This event provided a rare chance to validate our integrated model using local seismic records alone in the case of no coastal measurement. While the timing of simulated processes matches observations well, uncertainties in landslide volume remain a key factor influencing tsunami amplitude and coastal impact. The detailed seismic signals captured both near and far from the source shed light on the multi-stage dynamics of such cascading events and offer valuable input for improving hazard assessment in fjord-like environments.

1 Introduction

As climate is warming, coastal glaciers in Greenland have been retreating at unprecedented rates for 4 millennia (Meredith et al., 2019; Constable et al., 2022). The retreat of marine terminated glaciers in Greenland has various consequences for coastal biochemistry and ecosystems, including a reduction of nutrients and productivity once these glaciers have retreated inland

https://doi.org/10.5194/egusphere-2025-3803
Preprint. Discussion started: 18 September 2025

(Meredith et al., 2019). Moreover, glacier retreat in general has exacerbated the hazards associated with tsunamis: the emergence of new water areas, the release of constraints on nearby unstable slopes, the degradation of permafrost, and reduced freezing conditions all contribute to increased tsunami hazards in fjords depending on the geological context (Higman et al., 2015; Svennevig et al., 2020). In Polar Regions such as Greenland, such hazards can have important social consequences such as the temporary or permanent relocation of communities (Matti et al., 2023).

The 17th June 2017 landslide took place in the Karrat landslide complex, located on Ummiammakku Mountain in Karrat Fjord, which includes three landslide-prone areas (see map in Svennevig et al. (2020). The fjord includes several marine terminating glaciers but they are located upstream and did not play a role in this specific event. The 2017 event involved 58 million m^3 of material, including 45 million m^3 reaching the fjord and generating the tsunami (Gauthier et al., 2018). It is important to note that other events took place earlier; at least 3 rock avalanches were identified in 2009, 2016, and 2017 on the Karrat landslide complex using Sentinel 1 & 2, and Landsat imagery (Svennevig et al., 2020). Svennevig et al. (2020) suggest that permafrost melting due to climate change favors landslides on this type of steep and unstable slope. This type of event represents a threat to human life and has important social consequences. The huge landslide of 17th June 2017 led to a megatsunami, which devastated the village of Nuugaatsiaq 30 km away (Svennevig et al., 2020), and subsequently led to the decision to relocate people after the event (Matti et al. 2023).

Greenland's fjords, shaped by glacial erosion, feature steep walls and deep basins, making them particularly vulnerable to landslides and subsequent tsunamis. Typical fjords in Greenland vary in width from a few hundred meters to several kilometers, with depths often exceeding 500 meters and lengths of tens to hundreds of kilometers (e.g. Batcherlor et al., 2019). The steep topography combined with permafrost degradation increases the likelihood of large-scale mass movements, as seen in the Karrat Fjord landslide of 2017 (e.g. Svennevig et al., 2020). While detailed statistics on landslides in Greenland remain limited, the risk of similar events have been studied in the Uummannaq fjord system with retreating glaciers and unstable slopes (NGI, 2021). The first recorded tsunami triggered by a landslide is the 1952 Niiortuut landslide-tsunami event (Svennevig et al., 2023), which also had an associated single fatality and is attributed to permafrost degradation in western Greenland. More recently a tsunami-genic landslide on 16 September 2023 in an uninhabited fjord in East Greenland was also recorded on seismic networks globally (Svennevig et al., 2024; Carrillo-Ponce et al., 2024), while more local records have been found in lake sediments (Korsgaard et al., 2024). Glaciers and permafrost in Greenland have been experiencing a growing mass deficit in response to warming temperatures (Otosaka et al., 2023). There are consequently growing risks associated with climate-induced changes in Greenland's coastal and fjord environments.

This paper aims to demonstrate the potential of seismic monitoring to support a potential alert system on tsunamis in Fjord. Seismic monitoring has a long history in Greenland (e.g. Dahl-Jensen et al., 2010; Clinton et al., 2014) and the technique has been particularly used for glaciology (Veitch and Nettles, 2012; Walter et al., 2013; Röösli et al., 2017). The calving of icebergs can be recorded and analysed through seismograms (e.g. Sergeant et al., 2016) and geodetic observations for example (Nettles et al., 2008). Glacial earthquakes have also been detected seismically associated with both abrupt sliding of fast-moving ice streams as well as iceberg- (Joughin et al., 2008). A widespread seismic monitoring system would rely on the early detection of seismic waves induced by the ground motions due to the tsunami, as the velocity of these seismic waves is higher than the tsunami wave itself. To demonstrate the concept, we first analyse the seismic data at NUUG and argue that a signal due to the tsunami can be identified. Then we perform numerical modelling of the tsunami using the FUNWAVE hydrodynamic code. Finally, we model the ground deformation induced by this modelled tsunami in order to compare the modelled seismic waves with those we identified based on the seismic data at NUUG. Overall, our results demonstrate the concept, yet there are limitations discussed in section 4 and further research and developments would be needed before this concept can be effectively applied.

https://doi.org/10.5194/egusphere-2025-3803
Preprint. Discussion started: 18 September 2025

2. Method and model setting for the 2017 Landslide event

2.1 Seismic station at Nuugaatsiaq (NUUG)

On 17 June 2017, a huge landslide occurred in Karrat Fjord and led to a megatsunami that devastated the village of Nuugaatsiaq 30 km away (Schiermeier, 2017; Bessette-Kirton et al., 2018). The landslide was detected as an earthquake (71.640°N, 52.344°W, 0 km depth) equivalent to a magnitude of 4.2 and the origin time of the event was 23:39:12 in UTC (USGS, https://earthquake.usgs.gov/earthquakes/eventpage/us20009nlg/executive) (Fig. 1a). The source mechanism has been seismologically studied using the waveform inversions (Poli, 2017, Chao et al., 2018, Xie et al., 2020), and tsunami simulation has been carried out (Chao et al., 2018; Paris et al., 2019). Although there is no direct measurement of sea level rise during this tsunami event, several videos filmed by the inhabitants are available on YouTube (Underwood, 2017). It is estimated that the tsunami reached 1-1.5 m in height at Nuugaatsiaq and runup flooded up to 9 m in height (Strzelecki and Jaskólski, 2020). It is also reported from the field survey that tsunamis reached as high as 90 meters along the coastline on the same side as the landslide and 50 across the Karat Fjord near the landslide point (Georgia Institute of Technology, 2017). The seismic station NUUG in Nuugaatisaq (https://ds.iris.edu/ds/nodes/dmc/specialevents/2017/06/22/nuugaatsiaq-greenland-landslide-and-tsunami/) recorded the ground motions due to the landslide and probably the following tsunami (Fig. 1). We are particularly interested in the late oscillation (Fig. 1b) seen on a long period range. Chao et al. (2018) considered that this oscillation might have been generated in the middle of tsunami source and NUUG station due to the tsunami wave push to the coastline. Paris et al. (2019) considered that this might have been caused by the quasi-static sea level change near NUUG station. In general, the seismographs are useful to detect distant events as we explore in Section 3.1. As we will see, it is possible to determine the source parameters of seismic wave radiation immediately after the detection of signals, as the seismic waves generally propagate with a velocity of 3 km/s or higher for S-wave in the crust. On the other hand, tsunami waves may propagate with a velocity of tenths to hundreds of m/s according to the sea depth, briefly one-tenth of elastic wave velocity. Thus, this difference in travel time is used to give early warning of tsunami propagation at other locations globally. Thus, in the following, we demonstrate the complete tsunami process from the landslide radiating the seismic waves to the tsunami generation to discuss the long-period ground motion recorded at the seismic stations.

Figures 1b, 1c, and 1d show the UD displacement at the NUUG station with different frequency bands. We removed the DC offset and the instrumental response in advance. The top panel shows the high-pass filtered record at 0.001 Hz. It shows the harmonic signal with a period of 150 s starting about 400 s after the origin time of the landslide. This is the main response of tsunamis. The second panel shows the high-pass filtered record at 0.1 Hz. This high-frequency ground motion is reflected in the mass movement of the landslide and the generation of a tsunami. The bottom panel shows the band-pass filtered record at 0.02-0.1 Hz. It includes the main movement of the landslide, and smaller amplitude, which is the response of tsunami.

https://doi.org/10.5194/egusphere-2025-3803
Preprint. Discussion started: 18 September 2025

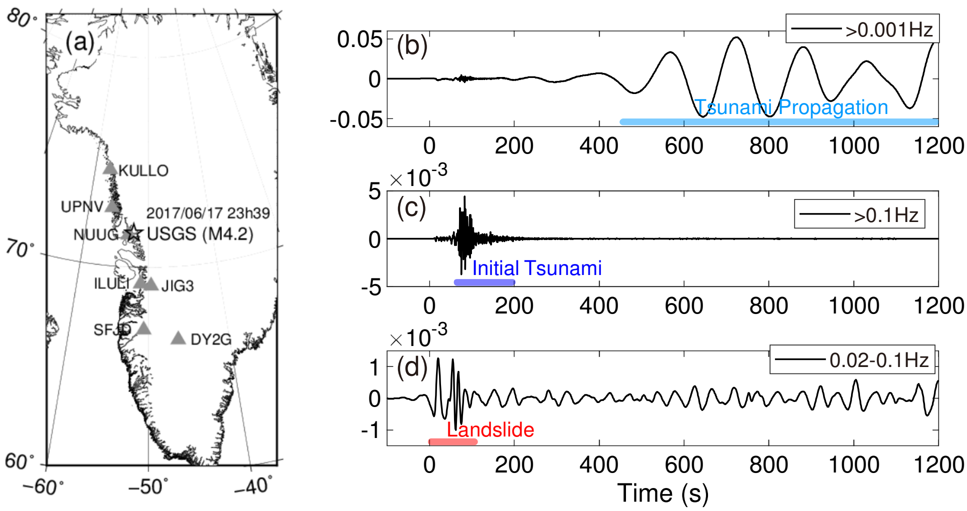

Figure 1: Map of the seismic stations and the UD displacement (in centimeters) at the NUUG station. (a) Map of stations used in this study. The open star shows the epicenter location of the landslide event determined by USGS and the gray triangles show the seismic stations. (b) high-pass filtered at 0.005 Hz, (c) high-pass filtered at 0.1 Hz, and (d) band-pass filtered at 0.02-0.1 Hz.

2.2 Simulation Strategy

The phenomena are complex from the landslide, tsunami, and solid earth deformation. However, each process goes on in different domains and different time scales so that one can treat them sequentially from one analysis to another. Figure 2 shows our simulation strategy for the whole phenomenon.

We start from a purely seismological approach of the single-force inversion with long-period seismic waveforms. We use the far-field regional stations in Greenland and then estimate the source time function and mass of the landslide. Second, we carry out a landslide simulation on the assumed slope, leading to the tsunami generation at the fjord. The results are then used as inputs into a simulation of the tsunami propagation through the fjords. Finally, the simulated seawater level change over the whole area is implemented in the ground motion simulation in the elastodynamic equations comparing to the static, analytical Boussinesq solution. Thus, each process is connected to the following steps.

Each process has different frequency ranges. The phenomena at high-frequency are influenced more by the detail of the model. Single-force inversion and oscillation simulation of the Earth need the crustal structure under the ground, and we adopt a simple 1D model from the generic model, as it is poorly known in the region. The near-surface complexity (surface topography or seawater layer), however, does not impact the seismic wave propagation at the frequencies that we are interested in. For the landslide simulation, the topography and the mass control are the primary controls on sliding into the sea. Finally, for the tsunami propagation simulation, the bathymetry is the most important parameter to correctly estimate the tsunami propagation speed. In the next chapter, we will explain in detail each step including the technical aspects and the results.

https://doi.org/10.5194/egusphere-2025-3803
Preprint. Discussion started: 18 September 2025

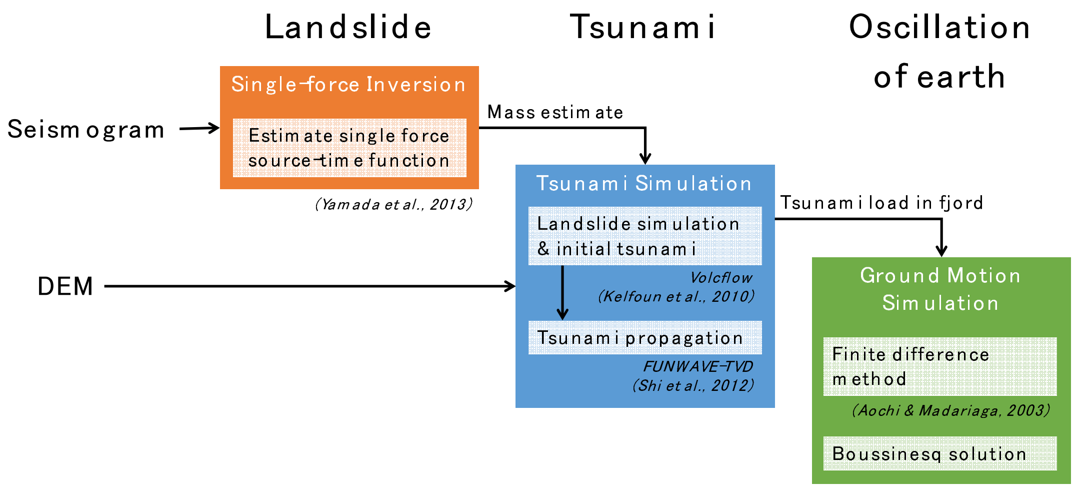

Figure 2: Simulation strategy for the 2017 landslide event.

3. Simulation Results

3.1 Single-force inversion from regional data

The kinematic inversion assuming a single-force mechanism is commonly deployed for landslides (e.g. Ekstroöm & Stark, 2013). Here, we use six seismic stations available on Greenland (Fig. 1a). We removed the closest NUUG station from this inversion since it is too close to apply the point-source approximation. The inversion was performed in the frequency domain with a limited frequency window (Nakano et al., 2008). The source is assumed to be a point source at the location of the landslide (52.34W, 71.64N, Depth 0km). We used the AK135 velocity structure to compute the Green's function (Kennett et al., 1995). The instrumental response was removed from the seismic records, and 4th-order Butterworth filter with corner frequencies of 0.02-0.1 Hz was applied. The detailed result is shown in Appendix A1. The obtained source time function (top panels of Figure S1 in Appendix) shows that the horizontal particle motion is dominant in the north-south direction, and the vertical component is larger than the horizontal component. The horizontal forces include the long-period noise. Based on the vertical component, the duration of the event is about 80 s. The maximum amplitude of the source time function is 0.2×10^{12} N. According to the scaling law in Ekström and Stark (2013), the mass is estimated as 0.11×10^{12} kg. Assuming an average rock density of 2.5×10^{3} kg/m^3, the total volume is roughly 44×10^{6} m^3 (see Section 3.2 for the comparison)

Figure 3 compares the synthetic and observed waveforms at NUUG and JIG3 stations. The synthetic waveforms are computed from the convolution between Green's function and the source time function of the inversion without the NUUG station. The waveform agreement is good at station JIG3 since this station is included in the inversion analysis. The synthetic waveforms at the NUUG station show a good fit on the vertical component. The horizontal components are more complex, probably because the detail of the local structure influences the wave propagation. We note a long-period signal at 100-250 s in the NS component, similar to the obtained source time function. The landslide may have been finished in about 100 seconds, while the signal force inversion detected the beginning of the tsunami generation (100-250 s), which reached up to 90 m (Georgia Institute of Technology, 2017). Although such phase is expected at the nearest NUUG station, we do not observe any corresponding phases in the NS component (Fig. 3). This is probably because this process applied on the EW-oriented coastline of the fjord, and while likely more visible at the far southern and northern stations was not visible at the NUUG station located to the west. This behaviour has not been reported in the previous analyses in the literature (Chao et al., 2018, Xie et al., 2020).

https://doi.org/10.5194/egusphere-2025-3803
Preprint. Discussion started: 18 September 2025

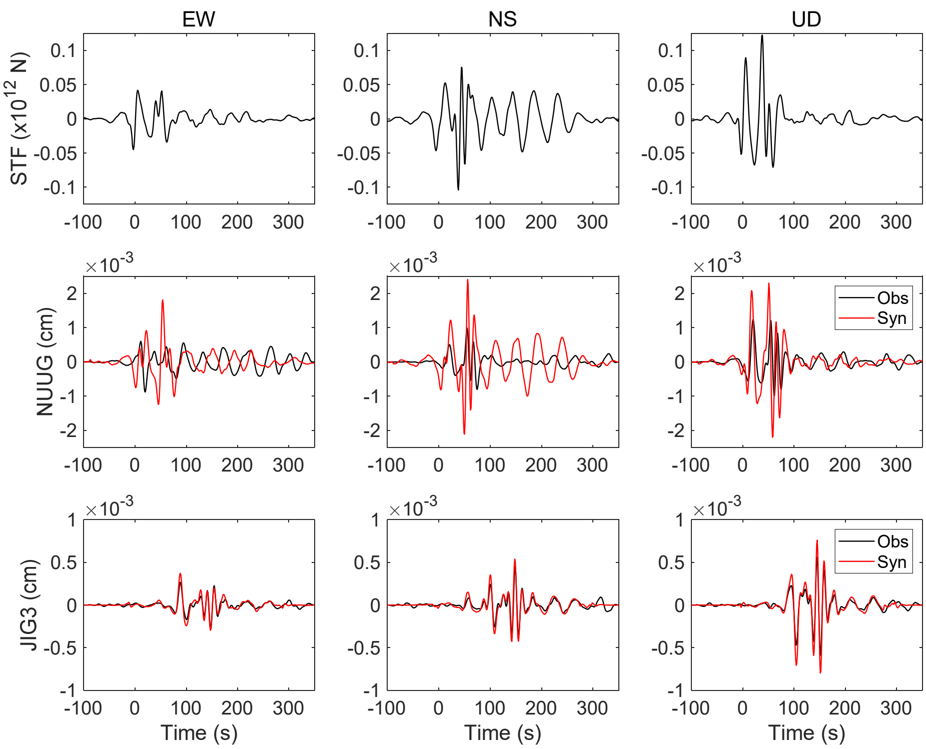

Figure 3: Source time function and waveform fitting. Top row: Source time function of the waveform inversion with the frequency of 0.02-0.1 Hz. Comparison between the observed (black) and synthetic (red) waveforms at NUUG station not included in the inversion (middle row) and JIG3 stations used in the inversion (bottom row). The X-axis shows the time after the origin of the landslide.

3.2 Simulation of tsunami generation and propagation

We performed a landslide tsunami simulation according to Mulia et al. (2020) by coupling the pyroclastic flow model, VolcFlow, with the Boussinesq wave model, FUNWAVE-TVD, using a 2-D numerical grid with a resolution of 100 meters. VolcFlow simulates both landslide dynamics and water flow using shallow water equations based on mass conservation and momentum equations (Kelfoun et al., 2010). It provides more accurate representations compared to static or rigid-body models, making it a valuable tool in landslide tsunami research (e.g., Giachetti et al., 2011, 2012). VolcFlow offers a cost-effective solution by capturing key 3-D interactions in a 2-D framework (Kelfoun et al., 2010). FUNWAVE-TVD is a fully nonlinear Boussinesq wave model designed to simulate a wide range of coastal processes, including wave propagation, shoaling, breaking, and shoreline dynamics. It accurately captures complex phenomena such as harbor resonance, infragravity waves, and sediment transport. Extensively validated through analytical, laboratory, and field studies, FUNWAVE-TVD has proven to be a reliable and versatile tool for coastal engineering and scientific research. Its adaptability makes it invaluable for understanding and addressing complex coastal dynamics.

We use the digital elevation model both for bathymetry and topography from GEBCO database (https://www.gebco.net/data_and_products/gridded_bathymetry_data/arctic_ocean/). VolcFlow was employed to simulate the

https://doi.org/10.5194/egusphere-2025-3803
Preprint. Discussion started: 18 September 2025

landslide and initial tsunami generation over a duration of 120 seconds. The simulations assumed an avalanche density of 2,500 kg/m³ and a water density of 1,027 kg/m³ to provide realistic environmental parameterization. To incorporate frequency dispersion effects during tsunami propagation, FUNWAVE-TVD was used to model wave dynamics starting from 120 seconds onward. This coupled modeling approach offers insights into both tsunami generation and propagation processes. The data and model are made available in Polar Stereographic projection coordinates (EPSG:3996, true scale set at 75°N) in meters. The horizontal datum for the data set is WGS 84 and the vertical datum is assumed to be Mean Sea Level (however, note there may be datum issues for older data, which can be to chart datum).

We adopt a landslide volume of 49.7 × 10^6 m^3, hereafter called as AP model, calculated by Paris et al. (2019). However, this is subject to uncertainty between 33.4 and 76 × 10^6 m^3 (Bassette-Kirton et al., 2017; Chao et al., 2018; Gauthier et al., 2018; Paris et al., 2019). We also compared the map and satellite images before and after the landslide and our estimation varied by a factor of 2. Figures 4 and 5 show snapshots of the landslide-induced tsunami generation until 120 seconds and the tsunami propagation after 120 seconds for the reference landslide volume (AP model). At about 500 seconds, we observe that the first tsunami wave front arrives in front of NUUG station and identify the coherent tsunami wavefront over the whole fjord width at the latest at 1000 seconds . The wave height in front of the NUUG station reaches about 0.7-0.8 m. Later, the tsunami wave field becomes more dissipative, and tsunami wavelength and width become smaller and more varied.

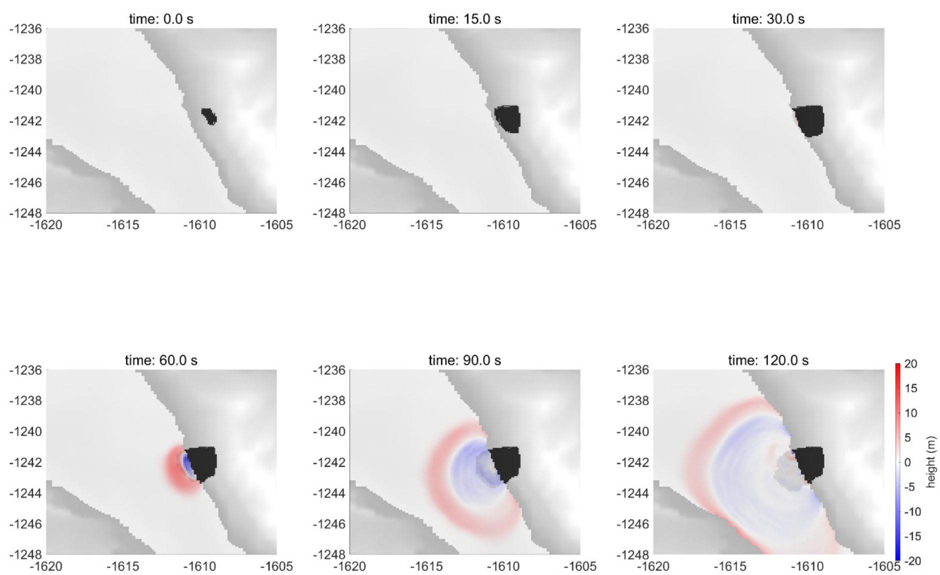

Figure 4: Snapshot of the simulation of landslide and tsunami generation. The black area indicates an ongoing landslide on the target slope. The landslide arrives at the sea at around 30 seconds. The generated tsunami height is shown in the colour bar in meters. The map uses the Polar Stereographic projection coordinates (EPSG:3996, true scale set at 75°N). The map scale is in kilometres.

https://doi.org/10.5194/egusphere-2025-3803
Preprint. Discussion started: 18 September 2025

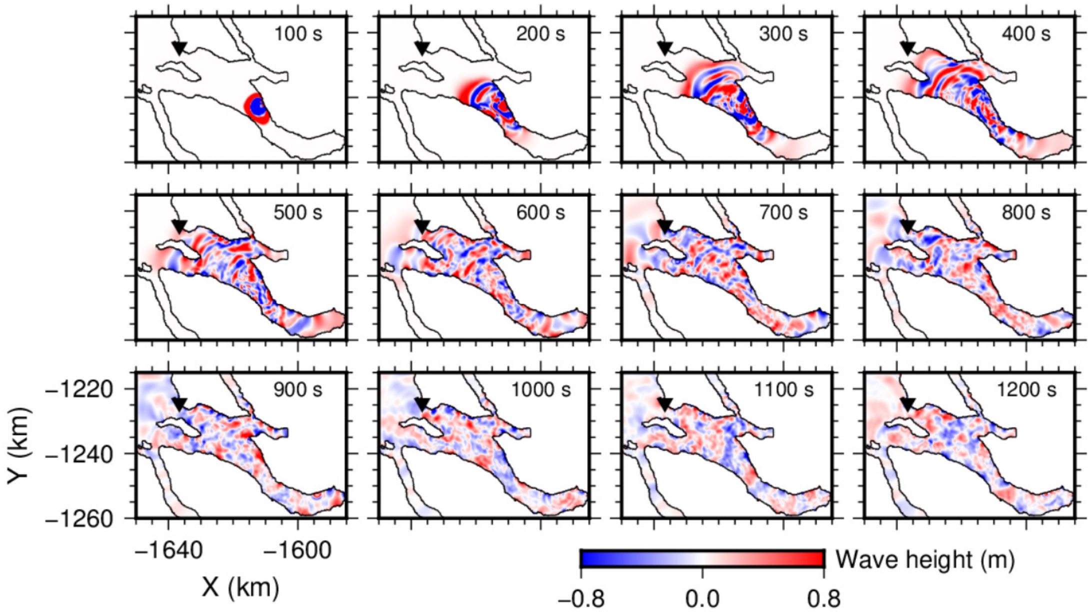

Figure 5: Snapshot of tsunami generation and propagation. The white area corresponds to the land above sea level. The triangle shows the position of NUUG. The map coordinates are the same as in Fig. 4.

3.3 Ground motion simulation on elastic media

Finally, we estimate the ground deformation at the NUUG station in Nuugaatsiaq. As shown in Figure 2, we adopt two approaches. One is based on the Boussinesq problem (See Supplementary Materials S2 and S3), which provides the analytical solution in a semi-finite elastic medium due to the vertical charge on the surface (Boussinesq, 1885). This solution or similar analytical solutions in the elastic medium are used for various geoscience applications to estimate the crustal deformation due to the surface charge and discharge (for example from ice sheets and glaciers, surface water reservoirs, mining exploitation, etc.) (e.g. Pinel et al., 2007; Bertinelli et al. (2008). On the other hand, we adopt a finite difference method (FDM) for calculating the ground deformation in space and time in the elastodynamic equation, where the seismic waves are propagating (e.g. Aochi & Madariaga, 2003). The seismic waves usually propagate with a speed of a few kilometers per second, followed by static deformation. For both approaches, we assume a homogeneous elastic medium with a rigidity μ = 34.1 GPa, corresponding to S-wave velocity of v_s = 3530 m/s, which is a typical value for crustal bedrock. The Boussinesq solution is calculated once per second using the tsunami height at the same time, while the FDM simulation is carried out with a time step of 0.005 seconds continuously from the beginning of the landslide simulation. The synthetics obtained from FDM are integrated once with respect to time to obtain the displacement.

Figure 6 compares the two approaches at the NUUG station position. Additional comparisons for simpler cases are given in Supplementary Material S4. Without a filter, the two estimations are very similar in displacement. First we do not to apply any filter on the simulated ground motions to be able to analyse the causality better (Fig. 6a). The first movement appears about 30 seconds after the landslide enters the sea. The body waves travel a distance of 30 km between the landslide site and NUUG station in about 5-10 seconds, so that the impact of this landslide process on the ground motions fades quickly within a minute. These effects are not significant in displacement and are consistent with the observation (Fig. 6b). Next, on the filtered ground motions (Fig. 6c), we observe an oscillation amplitude more important on the dynamic solution (FDM) than the static one (Boussinesq solution), although the observed amplitude is much larger (Fig. 6d). The impact of the tsunami wave

https://doi.org/10.5194/egusphere-2025-3803
Preprint. Discussion started: 18 September 2025

approaching the NUUG station becomes apparent after 400 seconds and periodic (mono frequency) oscillations are observed between 500 and 1200 seconds. These timings correspond to the passage of the tsunami wave near the station inferred from the snapshot of the tsunami propagation (Fig. 5).

Figure 7 presents the spatial distribution of the maximum displacement of the ground surface simulated by FDM. Here we apply a bandpass filter between 0.005 Hz and 0.01 Hz (100 – 200 seconds). We find that the vertical component of the ground motion is dominant, and larger than the horizontal components. We observe a displacement up to 0.01 cm along the coastline, attenuating with distance from the coast. We learn from this test that the tsunami can deform the surrounding solid earth and therefore the tsunami movement is detectable from a seismic station near the coastline. It should be visible in such fjord context in which the sear water level changes by an amplitude of 1 m with a wavelength of a few kilometres. The observed ground motions during the passage of the tsunami at NUUG were larger than the simulated ones; This may be, however, due to frequency limitation in the numerical simulations and uncertainty in the model parameters (see next section).

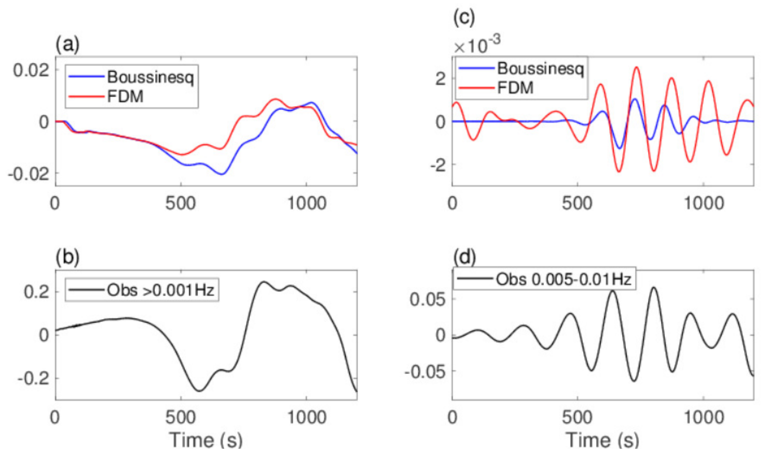

Figure 6: Comparison of the surface displacement calculated at Nuugaatsiaq, (X, Y)=(-1636.7 km, -1223.4 km). (a) Raw synthetic ground displacement in cm as calculated by the analytical Boussinesq solution and the FDM simulation. (b) Observed ground displacement in cm, lowpass filtered for 0.001 Hz. (c) Filtered synthetic ground displacement in cm from (a) at the bandpass window between 0.005 and 0.01 Hz. (d) Observed ground displacement in cm, filtered between 0.005 and 0.01 Hz.

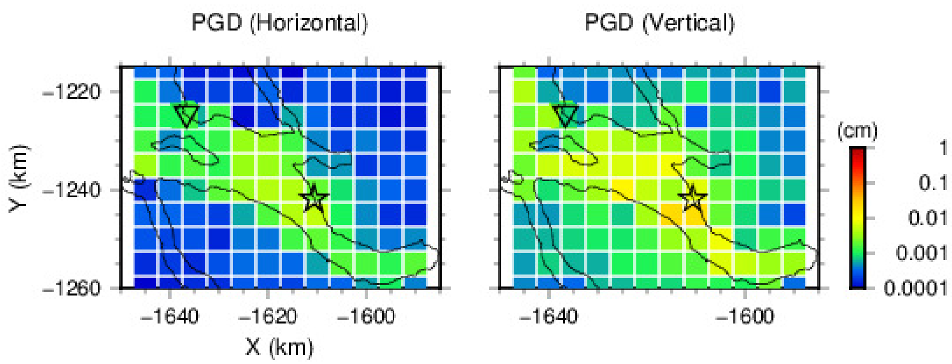

Figure 7: Spatial distribution of peak ground displacement (PGD), in the two horizontal components and the vertical (z) component, respectively. The synthetics are filtered between 0.005 Hz and 0.01 Hz. A star represents the landslide position and a triangle indicates the position of NUUG.

https://doi.org/10.5194/egusphere-2025-3803
Preprint. Discussion started: 18 September 2025

4. Discussion

4.1 Uncertainty in amplitude

We have conducted a chain of simulations which connect the occurrence of a landslide and the subsequent generation and propagation of a tsunami to the elastic ground deformation at the site of a seismic station (NUUG), located at a distance of 30 km from the landslide. While the simulated ground motions show good agreement in time with those recorded by the seismic station, the amplitude of the displacements is underestimated.

There are several possible reasons for this underestimation of ground motion amplitude. First, we estimated a quite high rigidity μ of the medium of 34.1 GPa. A lower rigidity is plausible, starting from 10 GPa, which corresponds to v_s = 2000 m/s. As the amplitude is proportional to $1/\mu$ (see supplementary material), an up to 3 times larger response could be expected.

Secondly, the estimation of landslide volume is uncertain to within a factor of 2. We carry out parameter studies for the landslide process by changing the volume (up to twice AP model) and the topography where the mass slides. Figure 8 compares the seawater change at Nuugaatsiaq during the tsunami passage for various landslide models (Table 1). The amplitude of sealevel change at Nuugaatsiaq becomes approximatively double (0.8 m in AP model to 1.6 m in APx2 model). On the other hand, the phase of the water level time series does not change significantly, since the timing of the tsunami generation process (when the landslide reaches the water and the first wave is generated) is unchanged. Since ground displacement is proportional to the instantaneous change in water level, an uncertainty factor of two in the water level amplitude implies an equal uncertainty factor in the ground displacement.

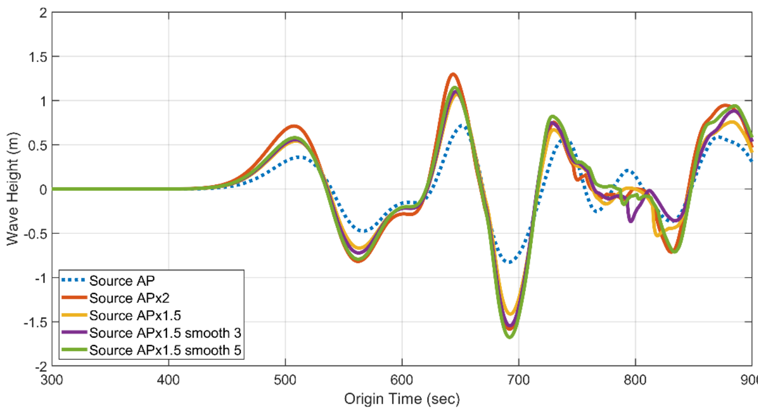

Figure 8: Comparison of the simulated coastal water levels during the tsunami passage at Nuugaatsiaq for different model parameters. The parameters and main results of the simulations are given in Table 1.

Case Name	**Landslide**	**Tsunami generation process**				**Tsunami at Nuugaatsiaq**		
	Volume ($\times 10^6$ m^3)	**Water Reach Time (sec)**	**First-wave*[1] Time (sec)**	**First half-period (sec)**	**Mass Stop Time (sec)**	**Wave Period (sec)**	**Max Wave Height (m)**	**Min Wave Height (m)**
A.P.	49.7	16	32	16	116	~130	0.72	-0.83
A.P. × 2	99.5	12	28	16	119	~130	1.3	-1.58
A.P. × 1.5	74.6	14	30	16	98	~130	1.07	-1.41

https://doi.org/10.5194/egusphere-2025-3803
Preprint. Discussion started: 18 September 2025

A.P. × 1.5 smooth3	74.6	14	32	18	117	~130	1.1	-1.54
A.P. × 1.5 smooth5	74.6	15	33	18	119	~130	1.14	-1.68

Table 1: Comparison of landslide models and main effects on the resulting simulated tsunamis at Nuugaatsiaq. (*[1]) indicates the time of the first negative wave appearing on the sea. It is worth noting that our seismological analysis gave a brief estimation of 44×10^{6} m^{3} for the landslide volume.

4.2 Comparison with other tsunami seismograms

There have been several cases in which the terrestrial geophysical instruments could detect the tsunami propagation. Nawa et al. (2007) analysed the records from pressure gauges and broadband seismometers in Antarctica for signals from the 2004 Indian Ocean tsunami generated by an earthquake in Sumatra. A tilt effect of several µGal (10^{-8} m/s^{2}) for about 0.2 m of sea water level change was observed at a frequency range between 0.3 and 0.6 mHz. Nishida et al. (2017) compared offshore pressure gauges and a broadband seismic station in the oceanic context for the 2015 Mw5.7 Torishima-oki tsunami earthquake. At a very low frequency range between 1.5 and 20 mHz, the ground velocity was about 1 to 10 µm/s for a tsunami height of about 2-5 cm. Tiltmeters can also be used to detect tsunami propagation. For example, during the 2010 Mw8.8 earthquake in Maule, Chile, tsunami propagation was detected by tiltmeters along the Chilean coastline (Boudin et al., 2013). The tilt response was about 0.05-0.01 µm at 7 km from the coastline for a sea level change of about 10 cm. The same tsunami was observed even along the Japanese coastline (Kimura et al., 2013, Kubota et al., 2020), with sea level anomalies of about 20-40 cm. This could be observed up to 50 km away from the coastline with about 5 x 10^{-3} µrad. Shaddox et al. (2021) reported, differently from tsunami, on the propagation of an internal gravity wave as detected by the broadband seismic station on Pratas Island in the South China Sea. Compared to these observations, the estimated tsunami height of the 2017 Karrat Fjord event was locally higher and the seismic stations are closer to the coastline (< 1km). Therefore, the ground oscillation could be clearly observed in broadband seismograms in velocity and displacement without the help of tiltmeters and gravimeters.

4.3 Implications for risk management

Cascading risks induced by climate change are explicitly considered in the 6th assessment report of the IPCC (Intergovernmental Panel on Climate Change), specifically in the Polar cross-chapter paper of the report of the working group II (Constable et al., 2022). However, the specific issue of tsunamis triggered by increasingly unstable slopes in a context of retreating glaciers is only implicitly considered, as part of a broad range of cascading impacts from climate change. We argue that it is important to recognize and assess this risk due to its potential to become a substantial threat to human life and key infrastructure. Mapping of existing landslide deposits in Western Greenland and inhabited parts of eastern Greenland is already underway (Svennevig, 2019). In addition, climate model projections—particularly those identifying areas vulnerable to permafrost thaw, whether currently or in the future—and the location of large calving glaciers provide valuable insights for assessing future hazard risks.

Our results show that the propagation of tsunamis in fjords can be effectively monitored in near real time using seismic data. This is relevant for arctic communities living close to fjords as it paves the way for the development of tsunami alert systems. To realize this potential, the concepts presented here should evolve toward an operational system, which requires advanced demonstration in real environments and validation. For example, future applied research and development projects could consist in demonstrating the concept on local sites, including by deploying adequate optical-fibre cables along coastlines. Concurrently, a systematic identification of coastal settlements concerned by this hazard will be essential to assess its importance and the need for alert system deployments.

https://doi.org/10.5194/egusphere-2025-3803
Preprint. Discussion started: 18 September 2025

Recent research has made substantial progress in the area of human settlements at risks from permafrost thaw and sea-level rise in the Arctic (Tanguy et al., 2024). Similar efforts could be undertaken to assess the potential of the threat from tsunamis to the settlements identified by Tanguy et al. (2024).

5 Conclusion

We conducted a comprehensive simulation chain of the cascading events on 17 June 2017 in Karrat Fjord, western Greenland—a large landslide, tsunami generation, and resulting ground deformation that tragically affected the village of Nuugaatsiaq. Using seismic records from seven stations across Greenland, we derived a source time function corresponding to a single-force model and estimated the landslide volume (~44×10^6 m³) through an empirical relation. This estimate falls within the range of previously published values. We then simulated the landslide descent and its interaction with the fjord water, followed by large-scale tsunami generation and propagation based on available topography and bathymetry. Ground deformation due to sea-level changes from the tsunami was also modeled and compared with seismic records at the NUUG station. This event provided a rare chance to validate our integrated model using local seismic records alone, in the absence of direct coastal measurements. Our results show that the timing of simulated signals aligns well with observations, confirming that both the landslide onset and the bathymetric data were appropriately represented. The predominant tsunami period was successfully captured, although later wave trains became less coherent due to multiple reflections within the fjord. Tsunami amplitude remains sensitive to uncertainties in the initial landslide volume. Ground deformation computed using both Boussinesq theory and 3D finite difference modeling showed consistent results, indicating that the tsunami-induced ground response is largely quasi-static. Simulated vertical displacements reached the millimeter scale for sea level changes of ~1 m—smaller than observed values at NUUG, likely due to uncertainties in subsurface rigidity and landslide parameters. Moreover, filtering of seismic records plays a critical role and can introduce artificial phases if not carefully applied. Finally, our study shows that tsunami propagation can be tracked along the coastline via seismic signals. Coupled modeling—from landslide dynamics to tsunami propagation and seismic response—offers detailed insights into the spatiotemporal evolution of such events. This approach can enhance tsunami hazard assessment in fjord environments and contribute to early warning capabilities. Seismic data, when combined with topographic and bathymetric information, can constrain landslide parameters and tsunami evolution in near real-time. Looking ahead, the deployment of optical-fiber sensing along coastlines or the seafloor could significantly improve our ability to monitor and understand similar cascading hazards, including glacier-related seismicity.

Data availability

Seismic data are available on Orfeus-EPOS (https://www.orfeus-eu.org/data/eida/, last accessed on the 28th January 2025). DEM data are available on GEBCO (https://www.gebco.net/data_and_products/gridded_bathymetry_data/arctic_ocean/, last accessed on the 28th January 2025).

Author Contribution

HA, MY, TCH, GLC brought principal conceptualization, and GLC ACH and RM brought the perspective of study. HA, MY and TCH brought data curation, analysis, methodology and validation, and HA and MY finalized visualization. GLC worked for funding acquisition and project administration. HA, MY and GLC prepared the manuscript with contributions from all co-authors.

https://doi.org/10.5194/egusphere-2025-3803
Preprint. Discussion started: 18 September 2025

Competing interests

The authors declare that they have no conflict of interest.

Acknowledgement

This study is a contribution to the PROTECT project in the framework of the European Union's Horizon 2020 research and innovation program under grant agreement 869304. We thank for all the collaborators especially from Asiaq Greenland Survey and Danish Metrological Institute. We also thank many colleagues from Geological Survey of Denmark and Greenland (GEUS). A part of the numerical study has been carried out on the French national supercomputing center GENCI/TGCC and GENCI/Idris under grants A0150406700 and A0170406700.

References

Aochi, H. and Madariaga, R.: The 1999 Izmit, Turkey, earthquake: Non-planar fault structure, dynamic rupture process and strong ground motion, Bull. Seism. Soc. Am., 93, 1249-1266, https://doi.org/10.1785/0120020167, 2003.

Batchelor, C. L., Dowdesell, J. A., Rignot, E., and Millan, R.: Submarine moraines in Southeast Greenland fjords reveal contrasting outlet-glacier behaviour since the last glacial maximum, Geophys R Lett, 46, 3279-3286. https://doi.org/10.1029/2019GL082556, 2019.

Bessette-Kirton, E., Allstadt, K., Pursley, J., and Godt, J.: Preliminary analysis of satellite imagery and seismic observations of the Nuugaatsiaq landslide and tsunami. USGS Landslide Hazards Program Website, Preliminary Assessments, https://www.usgs.gov/natural-hazards/landslide-hazards/science/preliminary-analysis-satellite-imagery-and-seismic (last acess: 26 March 2025), 2018.

Boudin, F., Allgeyer, S., Bernard, P., Hébert, H., Olcay, M., Madaraiga, R., El-Madani, M., Vilotte, J.-P., Peyrat, S., Nercessian, A., Schurr, B., Esnoult, M.-F., Asch, G., Nunez, I., and Kammenthaler, M.: Analysis and modelling of tsunami-induced tilt for the 2007, M=7.6, Tocopilla and the 2010, M=8.8 Maule earthquakes, Chile, from long-base tiltmeter and broadband seismometer records, Geophys J Int, 194, 269-288. https://doi.org/10.1093/gji/ggt123, 2013.

Bettinelli, P., Avouac, J.-P., Flouzat, M., Bollinger, L., Ramillien, G., Rajeure, S., and Sapkota, S.: Seasonal variations of seismicity and geodetic strain in Himalaya induced by surface hydrology, Earth Planet Sci Lett, 266, 332-344. https://doi.org/10.1016/j.epsl.2007.11.021, 2008.

Boussinesq, M. J.: Application des potentiels à l'etude de l'equilibre et du mouvement des solides elastiques – Gauthier-Villars, Paris, 1885.

Carrillo-Ponce, A., Heimann, S., Peterse, G. M., Walter, T. R., Cesca, S., and Dahm, T.: The 16 September 2023 Greenland Megatsunami: Analysis and modeling of the source and a week-long monochromatic seismic signal. Seismic Record, 4(3), 172-183, https://doi.org/10.1785/0320240013, 2024.

Chao W.-A., Wu T.R., Ma K.-F., Kuo Y.-T., Wu Y.-M., Zhao L., Chung M.J., Wu H. and Tsai Y.L.: The Large Greenland Landslide of 2017: Was a Tsunami Warning Possible? Seismol. Res. Lett., 89(4), 1335-1344. https://doi.org/10.1785/0220170160, 2018.

Clinton, J. F., Nettles, M., Walter, F., Anderson, K., Dahl-Jensen, T., Giardini, D., ... and Tsuboi, S.: Seismic Network in Greenland Monitors Earth and Ice System. *Eos, Transactions American Geophysical Union*, 95(2), 13–14. https://doi.org/10.1002/2014EO020001, 2014.

Constable, A.J., Harper, S., Dawson, J., Holsman, K., Mustonen, T., Piepenburg, D., and Rost, B.: Cross-Chapter Paper 6: Polar Regions. In: Climate Change 2022: Impacts, Adaptation and Vulnerability. Contribution of Working Group II to the Sixth Assessment Report of the Intergovernmental Panel on Climate Change [H.-O. Pörtner, D.C. Roberts, M. Tignor, E.S. Poloczanska, K. Mintenbeck, A. Alegría, M. Craig, S. Langsdorf, S. Löschke, V. Möller, A. Okem, B. Rama (eds.)]. Cambridge University Press, Cambridge, UK and New York, NY, USA, pp. 2319–2368, doi:10.1017/9781009325844.023, 2022.

Dahl-Jensen, T., Larsen, T. B. ., & Voss, P. H. (2010). Greenland ice sheet monitoring network (GLISN): a seismological approach. *GEUS Bulletin*, *20*, 55-58. https://doi.org/10.34194/geusb.v20.4956

Ekström, G. and Stark, C. P.: Simple scaling of catastrophic landslide dynamics, Science, 339, 1416-1419, https://doi.org/10.1126/science.1232887, 2013.

Fichtner, A., Hofstede, C., Kennett, B.L.N., Nymand, N.F., Lauritzen, M. L., Zigone, D., Eisen, O.; Fiber-Optic Airplane Seismology on the Northeast Greenland Ice Stream. *The Seismic Record,* 3 (2), 125–133, https://doi.org/10.1785/0320230004, 2023.

Gauthier, D., Anderson, S.A., Fritz, H.M. and Giachetti, T.: Karrat Fjord (Greenland) tsunamigenic landslide of 17 June 2017: initial 3D observations. Landslides, 15, pp.327-332, doi: 10.1007/s10346-017-0926-4, 2018.

Georgia Institute of Technology: After recon trip, researchers say Greenland tsunami in June reached 300 feet high. Homepage. Published on the 21th July 2017. https://www.ce.gatech.edu/news/after-recon-trip-researchers-say-greenland-tsunami-june-reached-300-feet-high (last accessed on the 26th March 2025), 2017.

Giachetti, T., Paris, R., Kelfoun, K. and Pérez-Torrado, F. J.: Numerical modelling of the tsunami triggered by the Güimar debris avalance, Tenerife (Canary Islands): Comparison with field-based data, Marine Geol., 284, 189-202, https://doi.org/10.1016/j.margeo.2011.03.018, 2011.

Giachetti, T., Paris, R., Kelfoun, K. and Ontowirjo, B.: Tsunami hazard related to a flank collapse of Anak Krakatau volcano, Sunda Strait, Indonesia, Geol. Soc. London., 361, 79-90, https://doi.org/10.1144/SP361.7, 2012.

Higman, B., Shugar, D.H., Stark, C.P., Ekström, G., Koppes, M.N., Lynett, P., Dufresne, A., Haeussler, P.J., Geertsema, M., Gulick, S. and Mattox, A.: The 2015 landslide and tsunami in Taan Fiord, Alaska. Scientific reports, 8(1), p.12993. https://doi.org/10.1038/s41598-018-30475-w, 2015.

Howat, I. M., Joughin, I., and Scambos, T. A.: Rapid changes in ice discharge from Greenland outlet glaciers, Science, 315, 159-1561. https://doi.org/10.1126/science.1138478, 2007.

Joughin, I., Howat, I., Alley, R. B., Ekstrom, G., Fahnestock, M., Moon, T., Nettles, M., Truffer, M. and Tsai, V. C.: Ice-front variation and tidewater behavior on Helheim and Kangerdlugssuaq Glaciers, Greenland, J. Geophys. Res., 113, https://doi.org/10.1029/2007JF000837, 2008.

Kelfoun, K., Giachetti, T., and Labazuy, P.: Landslide-generated tsunamis at Réunion Island, J. Geophys. Res., 115, F04012, https://doi.org/10.1029/2009JF001381, 2010.

Kennet, B.L.N., Engdahl, E. R. and Buland, R.: Constraints on seismic velocities in the Earth from traveltimes, Geophys. J. Int., 122, 108-124, https://doi.org/10.1111/j.1365-246X.1995.tb03540.x, 1995.

Kimura, T., Tanaka, S., and Saito, T.: Ground tilt changes in Japan caused by the 2010 Maule, Chile, earthquake tsunami, J Geophys Res, 118, https://doi.org/10.1029/2012JB009657, 2013.

Korsgaard N. J., Svennevig K., Søndergaard A. S., Luetzenburg G., Oksman M., and Larsen N. K.: Giant mid‐Holocene landslide‐generated tsunamis recorded in lake sediments from Saqqaq, West Greenland, Nat. Hazards Earth Syst. Sci. Discuss. 24, 757-772. https://doi.org/10.5194/nhess-2023-32, 2024.

Kubota, T., Saito, T., Chikasada, N. Y., and Suzuki, W.: Ultrabroadband seismic and tsunami wave observation of high-sampling ocean-bottom pressure gauge covering periods from seconds to hours, Earth Space Science, 7, e2020EA001197. https://doi.org/10.1029/2020EA001197, 2020.

Matti, S., Cullen, M., Reichardt, U. and Vigfúsdóttir, A.: Planned relocation due to landslide-triggered tsunami risk in recently deglaciated areas. International Journal of Disaster Risk Reduction, 86, p.103536, https://doi.org/10.1016/j.ijdrr.2023.103536, 2023.

https://doi.org/10.5194/egusphere-2025-3803
Preprint. Discussion started: 18 September 2025

Meredith, M., Sommerkorn, M., Cassotta, S., Derksen, C., Ekaykin, A., Hollowed, A., Kofinas, G., Mackintosh, A., Melbourne-Thomas, J., Muelbert, M.M.C., Ottersen, G., Pritchard, H. and Schuur, E.A.G.: Polar Regions. In: IPCC Special Report on the Ocean and Cryosphere in a Changing Climate [H.-O. Pörtner, D.C. Roberts, V. Masson-Delmotte, P. Zhai, M. Tignor, E. Poloczanska, K. Mintenbeck, A. Alegría, M. Nicolai, A. Okem, J. Petzold, B. Rama, N.M. Weyer (eds.)]. Cambridge University Press, Cambridge, UK and New York, NY, USA, pp. 203–320. https://doi.org/10.1017/9781009157964.005, 2019.

Mulia, I. E., Watada, S., Ho, T.-C., Satake, K., Wang, Y. and Aditiya, A.: Simulation of the 2018 tsunami due to the flank failure of Anak Krakatau volcano and implication for future observing systems. Geophys. Res. Lett., 47, e2020GL087334. https://doi.org/10.1029/2020GL087334, 2020.

Nakano, M., Kumagai, H. and Inoue, H. : Waveform inversion in the frequency domain for the simultaneous determination of earthquake source mechanism and moment function, Geophys. J. Int., 173, 1000-1011, https://doi.org/10.1111/j.1365-246X.2008.03783.x, 2008.

Nettles, M., Larsen, T. B., Elósegui, Hamilton, G.S., Steams, L. A., Ahlstrøm, A. P., Davis, J. L., Andersen, M. L., de Juan, J. Khan, S. A., Stenseng, L., Ekström, G. and Forsberg, R.: Step-wise changes in glacier flow speed coincide with calving and glacial earthquakes at Helheim Glacier, Greenland, Geophys. Res. Lett., 35, L24503, https://doi.org/10.1029/2008GL036127, 2008.

NGI: Hazard scenario simulations and 2017 event hindcast, project report for GEUS, N°20200823-01-R, available from https://www.geus.dk/Media/638140441113026078/NGI_20200823-01-R_Tsunami_Karrat.pdf, last accessed on the 26 March 2025), 2021.

Nishida, K., Maeda, T., and Fukao, Y.: Seismic observation of tsunami at Island broadband stations, J Geophys Res, 124, 1910-1928. https://doi.org/10.1029/2018JB016833, 2019.

Otosaka, I. N., Shepherd, A., Ivins, E. R., Schlegel, N.-J., Amory, C., van den Broeke, M., Horwath, M., Joughin, I., King, M., Krinner, G., Nowicki, S., Payne, T., Rignot, E., Scambos, T., Simon, K. M., Smith, B., Sandberg Sørensen, L., Velicogna, I., Whitehouse, P., A, G., Agosta, C., Ahlstrøm, A. P., Blazquez, A., Colgan, W., Engdahl, M., Fettweis, X., Forsberg, R., Gallée, H., Gardner, A., Gilbert, L., Gourmelen, N., Groh, A., Gunter, B. C., Harig, C., Helm, V., Khan, S. A., Konrad, H., Langen, P., Lecavalier, B., Liang, C.-C., Loomis, B., McMillan, M., Melini, D., Mernild, S. H., Mottram, R., Mouginot, J., Nilsson, J., Noël, B., Pattle, M. E., Peltier, W. R., Pie, N., Sasgen, I., Save, H., Seo, K.-W., Scheuchl, B., Schrama, E., Schröder, L., Simonsen, S. B., Slater, T., Spada, G., Sutterley, T., Vishwakarma, B. D., van Wessem, J. M., Wiese, D., van der Wal, W., and Wouters, B.: Mass Balance of the Greenland and Antarctic Ice Sheets from 1992 to 2020, Earth System Science Data Discussions, 1–33, https://doi.org/10.5194/essd-2022-261, 2022.

Paris, A., Okal, E. A., Guérin, C., Heinrich, Ph., Schindelé, F. and Hébert, H.: Numerical modeling of the June 17, 2017 Landslide and Tsunami Events in Karrat Fjord, West Greenland, Pageoph, 176, 3035-3057. https://doi.org/10.1007/s00024-019-02123-5, 2019.

Pinel, V., Sigmundsson, F., Sturkell, E., Geirsson, H., Einarsson, P., Gudmundsson, M. T., and Högnadóttir, T.: Discriminating volcano deformation due to magma movements and variable surface loads: Application to Katla subglacial volcano, Iceland, Geophys. J. Int., 169, 325-338. https://doi.org/10.1111/j.1365-246X.2006.03267.x, 2007.

Poli, P: Creep and slip: Seismic precursors to the Nuugaatsiaq landslide (Greenland), Geophys. Res. Lett., 44, 8832-8836, https://doi.org/10.1002/2017GL075039, 2017.

Rignot, E., Fenty, I., Menemenlis, D. and Xu, Y.: Spreading of warm ocean waters around Greenland as a possible cause for glacier acceleration, Annals Glaciology, 53(60). https://doi.org/10.3189/2012AoG60A136, 2012.

Röösli, C, Walter, F., Husen, S,, Andrews, L.C., Lüthi, M.P., Catania, G.A. and Kissling, E.: Sustained seismic tremors and icequakes detected in the ablation zone of the Greenland ice sheet. J. Glaciology. 60, 563-575. doi:10.3189/2014JoG13J210, 2014.

Schiermeier, Q.: Huge landslide triggered rare Greenland mega-tsunami. *Nature*. https://doi.org/10.1038/nature.2017.22374, 2017.

Sergeant, A., Mageney, A., Stutzmann, E., Montagner, J.-P., Walter, F., Moretti, L. and Castelnau O.: Complex force history of a calving-generated glacial earthquake derived from broadband seismic inversion, Geophys. Res. Lett., 43, http://doi.org/10.1002/2015GL066785, 2016.

Shaddox, H. R., Broadsky, E. E., Ramp, S. R., and Davis, K. A.: Seismic detection of oceanic internal gravity waves from subaerial seismometers, AGU Advanced, 2, e2021AV000475. https://doi.org/10.1029/2021AV000475, 2021.

Strzelecki, M. C. and Jaskólski, M. W.: Arctic tsunamis threaten coastal landscapes and communities – survey of Karrat Isfjord 2017 tsunami effects in Nuugaatsiaq, western Greenland, Nat. Hazards Earth Syst. Sci., 20, 2521–2534, https://doi.org/10.5194/nhess-20-2521-2020, 2020.

Svennevig, K.: Preliminary landslide mapping in Greenland, GEUS Bulletin, 43, https://doi.org/10.34194/GEUSB-201943-02-07, 2019.

Svennevig, K., Dahl-Jensen, T., Keiding, M., Merryman Boncori, J. P., Larsen, T. B., Salehi, S., Munck Solgaard, A., and Voss, P. H.: Evolution of events before and after the 17 June 2017 rock avalanche at Karrat Fjord, West Greenland – a multidisciplinary approach to detecting and locating unstable rock slopes in a remote Arctic area, Earth Surf. Dynam., 8, 1021–1038, https://doi.org/10.5194/esurf-8-1021-2020, 2020.

Svennevig, K., Keiding, M., Korsgaard, N. J., Lucas, A., Owen, M., Poulsen, M. D., Priebe, J., Sørensen, E. V., and Morino, C.: Uncovering a 70-year-old permafrost degradation induced disaster in the Arctic, the 1952 Niiortuut landslide-tsunami in central West Greenland, Science of The Total Environment, 859, 160110, https://doi.org/10.1016/j.scitotenv.2022.160110, 2023.

Svennevig, K., Hicks, S. P., Forbriger T., et al. : A rockslide-generated tsunami in a Greenland fjord rang Earth for 9 days, Science, 385, 1196-1205, https://doi.org/10.1126/science.adm9247, 2024.

Tanguy, R., Bartsch, A., Nitze, I., Irrgang, A., Petzold, P., Widhalm, B., et al.: Pan-Arctic assessment of coastal settlements and infrastructure vulnerable to coastal erosion, sea-level rise, and permafrost thaw. *Earth's Future*, 12, e2024EF005013. https://doi.org/10.1029/2024EF005013, 2024.

Underwood, E.: What precursors foretold Greenland's recent 100-meter tsunami?, *Eos, 98*, https://doi.org/10.1029/2017EO085499, 2017.

Veitch, S. A., and Nettles, M.: Spatial and temporal variations in Greenland glacial-earthquake activity, 1993–2010. *Journal of Geophysical Research: Earth Surface*, 117(F4). https://doi.org/10.1029/2012JF002412, 2012.

Walter F., Olivieri M., and Clinton J.F.: Calving event detection by observation of seiche effects on the Greenland fjords. *Journal of Glaciology*. 59, 162-178. doi:10.3189/2013JoG12J118, 2013.

Xie, H. J., Chu, R., and Ni, S.: Relocation of the 17 June 2017 Nuugaatsiaq (Greenland) Landslide based on Green's functions from ambient seismic noises, J Geophys Res, 125, e2019JB018947, https://doi.org/10.1029/2019JB018947, 2020.